

Characterization of Arbuckle-basement wastewater disposal system, Payne County, Northern Oklahoma

Gabriel L. Machado¹, Garrett J. Hickman¹, Maulin P. Gogri¹, Kurt J. Marfurt¹, Matthew J. Pranter¹, and Zulfiquar A. Reza¹

Abstract

Over the past eight years, north-central Oklahoma has experienced a significant increase in seismicity. Although the disposal of large volumes of wastewater into the Arbuckle Group basement system has been statistically correlated to this increased seismicity, our understanding of the actual mechanisms involved is somewhat superficial. To address this shortcoming, we initiated an integrated study to characterize and model the Arbuckle-basement system to increase our understanding of the subsurface dynamics during the wastewater-disposal process. We constructed a 3D geologic model that integrates 3D seismic data, well logs, core measurements, and injection data. Poststack-data conditioning and seismic attributes provided images of faults and the rugose top of the basement, whereas a modified-Hall analysis provided insights into the injection behavior of the wells. Using a Pareto-based history-matching technique, we calibrated the 3D models using the injection rate and pressure data. The history-matching process showed the dominant parameters to be formation-water properties, permeability, porosity, and horizontal anisotropy of the Arbuckle Group. Based on the pressure buildup responses from the calibrated models, we identified sealing and conductive characteristics of the key faults. Our analysis indicates the average porosity and permeability of Arbuckle Group to be approximately 7% and 10 mD, respectively. The simulation models also showed pockets of nonuniform and large pressure buildups in these formations, indicating that faults play an important role in fluid movement within the Arbuckle Group basement system. As one of the first integrated investigations conducted to understand the potential hydraulic coupling between the Arbuckle Group and the underlying basement, we evaluate the need for improved data recording and additional data collection. In particular, we recommend that operators wishing to pursue this type of analysis record their injection data on a daily rather than on an averaged basis. A more quantitative estimation of reservoir properties requires the acquisition of P-wave and dipole sonic logs in addition to the commonly acquired triple-combo logs. Finally, to better quantify flow units with the disposal reservoir, we recommend that operators acquire sufficient core to characterize the reservoir heterogeneity.

Introduction

According to The Office of the Secretary of Energy and Environment (Oklahoma), the state of Oklahoma has experienced limited but consistent levels of seismicity in the recorded history dating back to 1882 (earthquakes.ok.gov). However, north-central Oklahoma has experienced a recent and dramatic rise in the number of earthquake events. This cannot be solely attributed to natural causes. Walsh and Zoback (2015) provide a discussion of the increase in seismicity (Figure 1). They mention that no other state has witnessed an increase in seismicity as much as Oklahoma in recent years. Jacobs (2016) reports more than 2500 seismic events with >2.5 Richter magnitude between 2010 and 2015 in Oklahoma.

Multiple studies including but not limited to Zoback (2010), Horton (2012), Kim (2013), McGarr et al. (2015), and Walters et al. (2015) indicate that the seismicity is linked to wastewater disposal. To address this issue, the Oklahoma Corporation Commission implement a “stoplight” plan of action that required the reduction (a yellow light) or cessation (a red light) of injected wastewater volumes. Since the plan has been implemented, there has been a reduction in earthquakes exceeding a magnitude of three or greater from 903 in 2015 to 623 in 2016, 302 in 2017, and 196 in 2018 (Tulsa World, 2019). This decrease in seismicity occurred when the volume of oil produced increased from 166 MMBBL in 2015 to 192 MMBBL in 2018 (EIA, 2019). The increased cost of wastewater disposal, public relations

¹University of Oklahoma, Norman, Oklahoma, USA. E-mail: gmachado@ou.edu; garrett.hickman@ou.edu; maulingogri@ou.edu; kmarfurt@ou.edu; matthew.pranter@ou.edu; zulfiquar.reza@ou.edu.

Manuscript received by the Editor 22 February 2019; revised manuscript received 5 July 2019; published ahead of production 03 September 2019; published online 15 October 2019. This paper appears in *Interpretation*, Vol. 7, No. 4 (November 2019); p. SL19–SL36, 27 FIGS., 2 TABLES. <http://dx.doi.org/10.1190/INT-2019-0025.1>. © 2019 Society of Exploration Geophysicists and American Association of Petroleum Geologists. All rights reserved.

concerns, and new exploration opportunities have shifted oil and gas production from the high water-cut Mississippian Limestone play of north-central Oklahoma (e.g., [Matson, 2013](#)) to the lower water-cut STACK and SCOOP plays of central and south-central Oklahoma ([Pickett, 2018](#)). Outside of Oklahoma, hydraulic-fracturing operations have been attributed to be the primary cause of induced seismicity ([British Columbia Oil and Gas Commission, 2011](#); [Holland, 2013](#); [Friberg et al., 2014](#); [Walters et al., 2015](#)). Although several seismic events in Oklahoma have been linked to hydraulic-fracture stimulation ([Holland, 2013](#)), none have been reported in north-central Oklahoma where most seismic events have occurred and where our study focuses. Therefore, this study does not focus on hydraulic-fracture-induced seismicity.

The United States Environmental Protection Agency (EPA) designates class II wells as those used to inject fluids associated with oil and gas into the subsurface. In general, permeable formations are the target of class II wells. According to the [U.S. Geological Survey \(2019\)](#), 40,000 out of 150,000 class II wells operating in the USA are used for oil and gas wastewater (primarily brine) disposal. Other class II wells include those used for enhanced recovery and hydrocarbon storage. The total produced water volume in the USA exceeded 20 billion stock-tank barrels (STB) in 2007 as reported by [Clark and Veil \(2009\)](#). Enhanced recovery operations consumed more than 55% of this water, whereas approximately 39% of the water was disposed of through wastewater injection wells. A small fraction of these disposal wells has caused induced seismicity, thereby triggering a large concern among the public and governmental organizations. This increase in seismicity has led federal and state bodies to find ways to mitigate the risk of induced seismicity. The State of Oklahoma Underground Injection Control division recognizes three necessary components for significant injection-induced seismicity: (1) sufficient pressure buildup from disposal activities, (2) the presence of faults, and (3) a pathway allowing the increased pressure to communicate with the faults.

Resource plays such as the Mississippian Limestone of Oklahoma and Kansas are characterized by up to

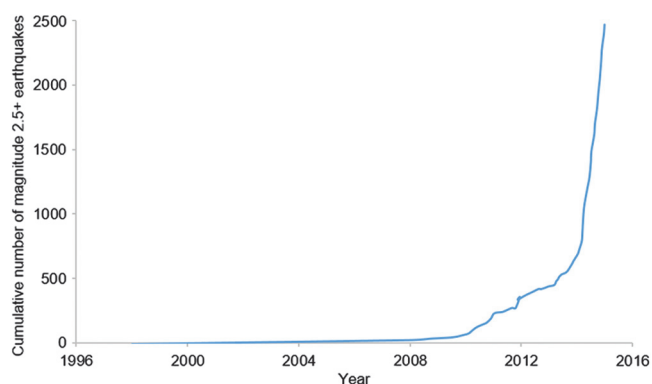


Figure 1. Cumulative number of magnitude 2.5+ earthquakes in Oklahoma (after the study by [Walsh and Zoback, 2015](#)).

95% hypersaline water production. Although the entire state of Oklahoma has thousands of water disposal wells, it is only north-central Oklahoma that has experienced a recent increase in seismicity. [Walsh and Zoback \(2015\)](#) state that in north-central Oklahoma, most wastewater is disposed of in the high-porosity, high-permeability, and often karsted Arbuckle Group. In addition, these authors hypothesize that this formation is in hydraulic communication with the underlying crystalline basement. Increases in pressure in the Arbuckle Group are transmitted into the basement, thereby modifying the ambient stress field and facilitating slippage along the preexisting zones of weakness. The exact details of such pressure transmission are unknown, with some scientists suggesting fluid flow into the basement along faults and others proposing a somewhat simpler loading process.

Although various authors have established spatiotemporal correlations between wastewater injection and earthquakes across the USA and other countries ([Evans, 1966](#); [Walsh and Zoback, 2015](#); [van der Baan and Calixto, 2017](#)), there is still a poor understanding of the mechanisms of earthquake triggering in north-central Oklahoma. However, one aspect is clear: that geologic variability controls the occurrence of such events and basement rocks in Oklahoma and is not homogeneous ([Elebiju et al., 2011](#); [Chopra et al., 2018](#); [Kolawole et al., 2018](#)). To further investigate these issues, data for this study include modern wide-azimuth 3D seismic data volumes, well logs, and injection volumes in Payne County, Oklahoma. These data were used to provide a better understanding of the subsurface geology and ideally, insight on how to mitigate future seismic events. We conduct, to our knowledge, the first integrated, multidisciplinary characterization study of the Arbuckle Group-basement wastewater disposal system.

We begin our paper with a review of the geologic setting and the data available, followed by a summary of our three-step data-integration workflow. The first step includes establishing the structural and stratigraphic framework for the basement, Arbuckle Group, and overlying strata and constructing a 3D reservoir model of the subsurface geology. The second step includes correcting and analyzing the injection-well data. The third step includes history matching where we evaluate whether key faults act as fluid conduits or seals and we also discuss some of the limitations for the methodology presented. Each of these steps required perturbing the other two steps. We conclude with a summary of our results: a discussion of the strengths and weaknesses of our analysis and a list of conclusions including recommendations for data acquisition for improved wastewater reservoir characterization studies.

Geologic setting

The Arbuckle Group of central and northern Oklahoma was deposited during the Cambrian and Ordovician as an extensive carbonate platform that covered most of the region. Strata in the study area are 100s to 1000s of feet thick and were altered, in part, by

fracturing, dolomitization, and karstification processes. Cambrian and Ordovician carbonates are underlain by 50–100 ft of interbedded sandstones and dolomites of the Reagan Sandstone (Stringer, 1958), which in turn lies upon faulted Pre-Cambrian/Cambrian granites and rhyolites that form the shallow part of the basement throughout much of Oklahoma (Johnson, 1991). The heavily fractured and karsted carbonate formations have been the main disposal units for salt-water disposal wells throughout much of Oklahoma (Murray, 2015).

Data used

Figure 2a shows the location of Payne County in Oklahoma. The availability of a modern 3D seismic survey imaging the Arbuckle Group and basement along with other overlying formations was a key factor in selecting the study area. Figure 2b shows the location of 29 wastewater disposal wells penetrating the Arbuckle Group in the study area. Figure 2c shows a chair display through the seismic amplitude volume. Obtaining modern 3D seismic data for a study related to induced seismicity can be difficult. As an active player (and generator of wastewater), the operator of this area was motivated to provide a data license to better understand the subsurface complexity and devise disposal techniques to mitigate any potential risk of seismicity. Because they are actively developing the shallower objectives, the license agreement proscribed the display of seismic data above the top Arbuckle Group. Well-log data includes digitized raster logs for 29 wells that penetrate the Arbuckle Group for a depth range of 3000–6000 ft (914–1282 m). Log curves include gamma ray (GR), bulk density (RHOB), neutron porosity (NPHI), density porosity (DPHI), spontaneous potential, shallow resistivity (RESS), medium resistivity

(RESM), and deep resistivity (RESD). Sonic or velocity logs were not available. Various data were available from the Amoco No. 4 Shads, slim-hole cored well, Rogers County, Oklahoma (70 mi to the east — northeast of the study area), which was drilled to basement. Data include porosity, permeability, grain density, mineralogy using Fourier transform infrared spectroscopy, and sonic velocities. Figure 3 shows the depth ranges of the seven cored intervals and the related formations.

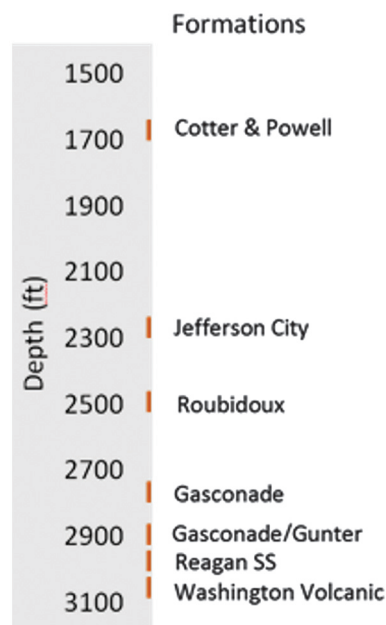


Figure 3. Core from the Catoosa, OK, Amoco Shads no. 4 well, with its formations and their respective depths, located approximately 15 mi from the study area (Gogri, 2018).

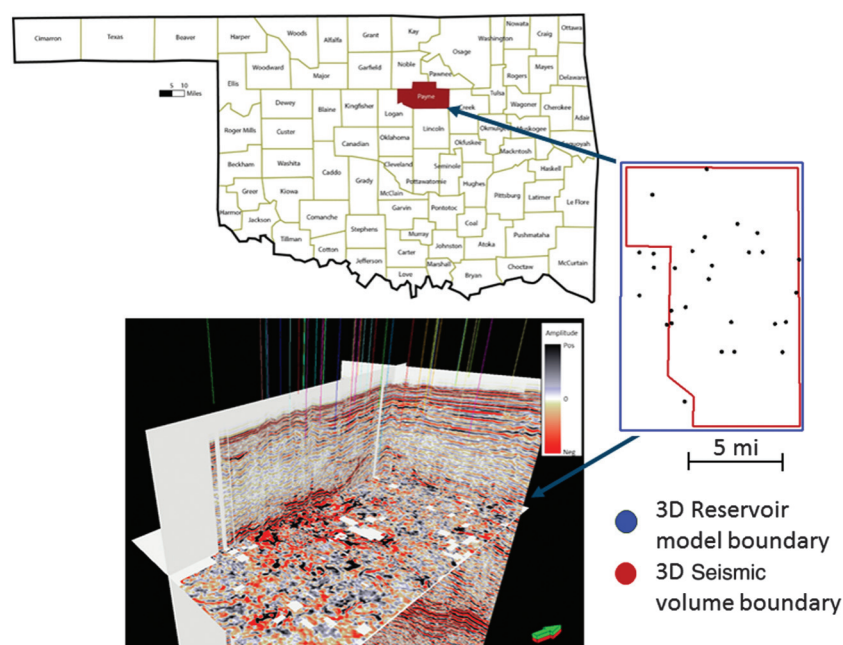


Figure 2. (a) Map showing the location of Payne County, Oklahoma. (b) Boundaries (in crimson) of the 3D seismic survey and (in blue) of the 3D cellular model. The black dots indicate the wells that penetrated the Arbuckle in the study area. (c) A chair display through the seismic amplitude volume. The top of the survey has been cropped 20 ms above the top Arbuckle Formation. The time slice is approximately 800 ms below the top of the basement.

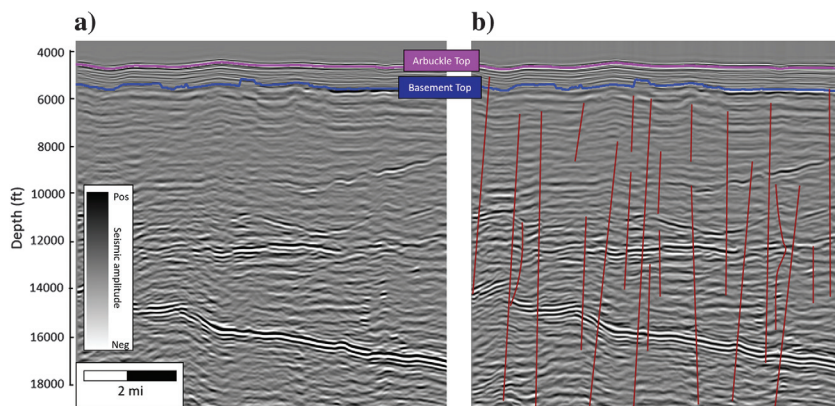


Figure 4. Vertical slice through the 3D seismic amplitude volume (a) before and (b) after structural-oriented-filtering and spectral balancing with a -114° phase shift as guided by the data owner. The red sub-vertical lines are example faults interpreted in the basement.

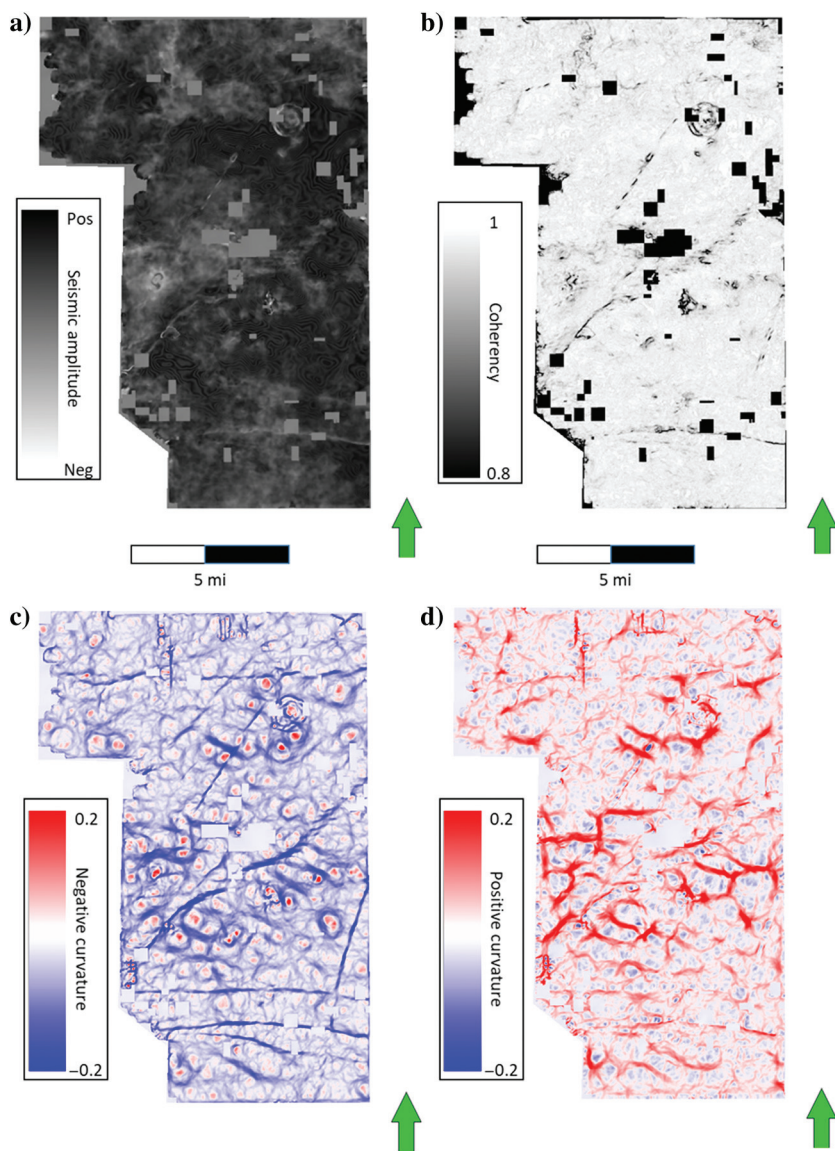


Figure 5. Horizon slice of the Arbuckle Group top through (a) seismic amplitude, (b) coherence, (c) negative curvature, and (d) positive curvature.

Methods

Our first objective was to construct a stratigraphic and structural framework consistent with our understanding of the stratigraphic and tectonic history of the area that honored the well-log, core, and 3D seismic data.

3D seismic processing, interpretation, and attribute analysis

We processed and interpreted a wide-azimuth, high-fold, 3D-seismic survey acquired in Summer 2014 using state-of-the-art processing techniques, including modern surface-consistent statics, careful velocity analysis, and prestack time migration to optimally focus on the shallower Mississippi Lime and Red Fork exploration targets. The image of the deeper, stratigraphically complex but tectonically simple Arbuckle Group is excellent, whereas that of the still deeper more structurally complex basement is suboptimal. Without access to the original shot gathers at the time, we were unable to reprocess the data using prestack depth migration to account for the lateral velocity variation of the overburden (Figure 4a). Nevertheless, we were still able to improve the signal-to-noise ratio (though not the focusing and position) of these deeper reflectors using a structure-oriented filter to remove noise components cutting across the structural dip, along with spectral balancing. Next, guided by the data owner, we applied a phase shift of -114° to properly allocate reflectors sign to the corresponding lithologies (Figure 4b).

A suite of different seismic attributes was computed to characterize the system, using the software developed at the University of Oklahoma (AASPI, 2017). Figure 5 shows a suite of horizon slices through three of the attributes that proved to be most useful in mapping structural features along the top Arbuckle Group.

Coherence, which normally delineates faults that exhibit finite reflector offset, is the workhorse of most modern 3D seismic structural interpretation workflows (Bahorich and Farmer, 1995; Chopra and Marfurt, 2007). However, in this study, the resulting images were disappointing because the chaotic nature of the basement does not permit for faults to be clearly delineated by this

attribute (Figure 5b). Along the top Arbuckle and top basement where the seismic image quality is excellent, the fault displacements are either too small, or alternatively, too smeared (where the displacement is distributed by conjugate faults over a finite zone) to be delineated by coherence. Curvature provided a better delineation of some faults (Figure 5c and 5d). An alternative geologic interpretation is that many of these faults are strike-slip in origin, where the deformation is accommodated by Riedel shears and flexures that exhibit little vertical offset, forming a fault damage zone.

In contrast to coherence, structural curvature “sees” such smeared images as a flexure (Figure 5c and 5d). Numerically, curvature is defined in two dimensions as the inverse of the radius of a circle tangent to and fitting a curve, with anticlines having positive curvature and synclines having negative curvature. Planar features exhibit zero curvature (Chopra and Marfurt, 2007). For a normal fault, the footwall will exhibit a positive curvature anomaly (an antiform), whereas the hanging wall will exhibit a negative curvature anomaly (a synform). In general, these two curvature anomalies will bracket a normal fault. Analyzing the strike-slip El Reno Fault 65 mi west of the study area, Liao et al. (2017) find that curvature could delineate not only Riedel shears but also a suite of rhombochasm forming a wide damage zone. Most-positive curvature will delineate the axis of upthrown structures.

Aberrancy measures the lateral change (or gradient) of curvature along an interpreted or inferred surface. Whereas curvature anomalies will bracket a fault, aberrancy will track the coherence anomaly and fall between the most-positive curvature anomalies defining the footwall and the most-negative curvature anomalies defining the hanging wall. For this reason, aberrancy can delineate faults whose throw falls below the seismic resolution (Qi and Marfurt, 2017). Aberrancy is the third derivative of the structure, highlighting discontinuities with a small vertical displacement. We can use this attribute to further characterize discontinuities by their azimuthal orientation (Figure 6). The seismic azimuth is perpendicular ($\pm 90^\circ$) to the geologic strike and defined as 0° from the north, increasing in the clockwise direction to a maximum of 359° ; e.g., if the structural strike of a seismic feature is east–west dipping to the south, its corresponding azimuth is 180° .

In general, seismic attributes such as coherence, curvature, and aberrancy provide excellent images of subtle features in well-imaged seismic data volumes. In contrast, deeper within the basement, prestack time-migration operator aliasing artifacts and misalignment of reflectors with fault edges make most attribute analyses difficult.

Well-log cross sections and formation correlation

Well-log data were used to interpret formation tops and to create a grid of structural and stratigraphic cross sections. The interpreted formations included the

Ordovician Arbuckle Group through the Pennsylvanian Oolagah (“Big Lime”) Formation (Figure 7). Structure-contour and isopach maps were generated for the Arbuckle Group and each of the other overlying sedimentary formations.

Structure-contour and isopach mapping

We created structure-contour maps (surfaces) for the formations that overlie the Arbuckle Group using only interpreted well-log tops. We could not use 3D seismic data for these overlying formations due to restrictions based on the seismic licensing agreement. We constructed the structure-contour map for the top of Arbuckle Group from both formation tops in 29 wells and the corresponding depth-converted seismic horizons using least-squares to fit the seismic horizon trend to the well tops map. We followed a similar approach for the top of the basement. In this case, however, because there was no marker for the basement in most wells because it is not an exploration target, we assumed that for each well, the drilling stopped once the basement rock was hit. With this, we approximated the depth of the basement to the true depth of the wells. Figure 8 shows that the surface constructed for the Arbuckle Group top is structurally highest in the northeast and

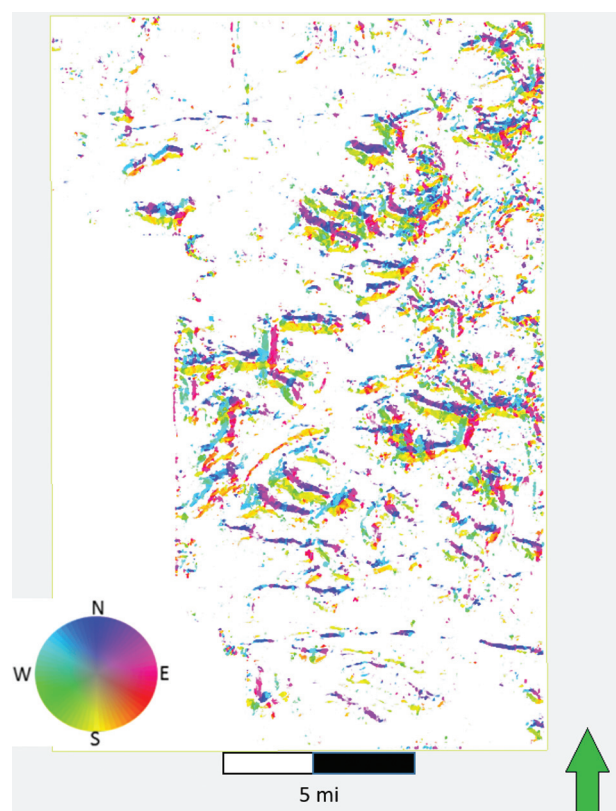


Figure 6. Time slice at the approximate location of the Arbuckle Group top through total aberrancy corendered with the azimuth of the aberrancy. An opacity curve is applied such that high aberrancy features appear transparent. Events are colored according to the azimuth in which they flex downward.

dips toward the southwest. We also constructed an isopach map for the Arbuckle Group by subtracting the basement top depths from the Arbuckle top depths.

Construction of a 3D reservoir model

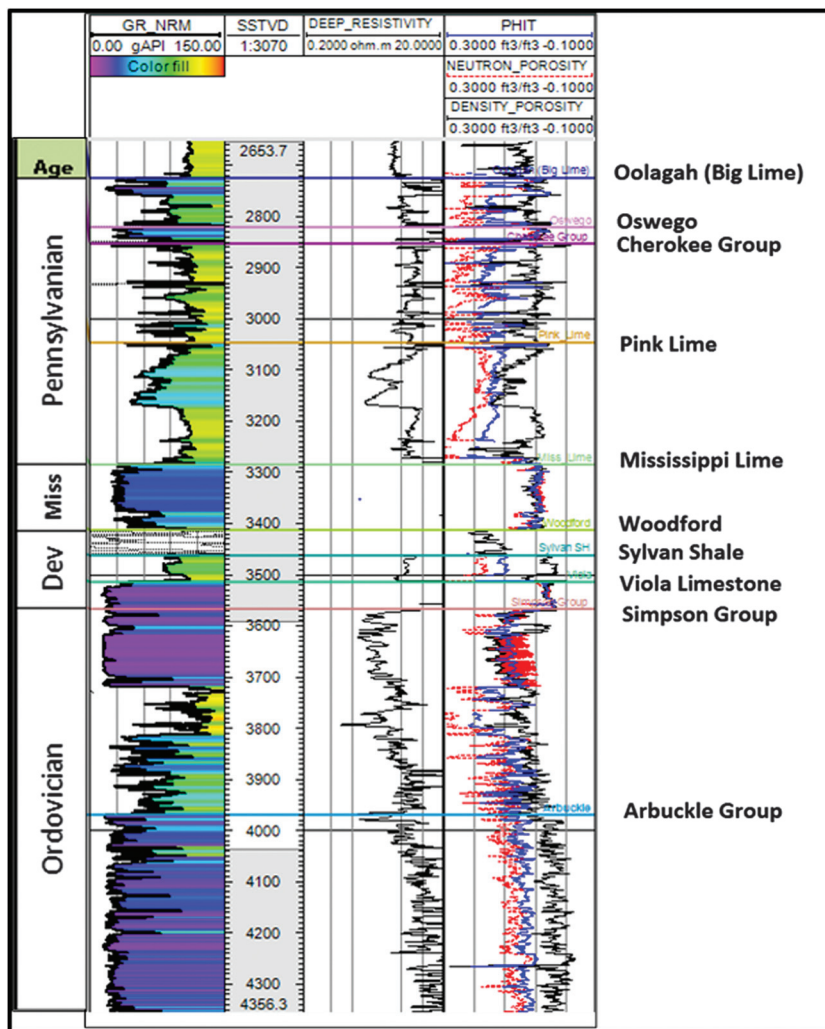
Interpreted faults (or fault surfaces) from the 3D seismic data do not exhibit significant vertical offset; therefore, we did not explicitly include them in the 3D reservoir model grid. However, we subsequently mapped porosity trends using the fault surfaces within the Arbuckle-basement interval and included the faults in the fluid-flow simulation model for calibration. We included a part of the basement (500 ft or 152.4 m thick interval) in the 3D simulation grid below the Arbuckle Group. The choice for the 500 ft interval of basement in the model was due to the lack of well log deep into the basement, and also because we do not expect pressure effects to extend too deep into the basement. We included the Arbuckle Group, as well as the Simpson and Viola Formations in the 3D reservoir model grid based on the interpreted surfaces. The 3D grid consists of cells with aerial dimensions of 500 × 500 ft (152 × 152 m) and an average layer thickness of 3 ft

(0.9 m) resulting in a total of approximately 6.5 million cells.

Porosity modeling

Upscaled total porosity logs (based on neutron and density porosity logs) and variogram parameters constrained the 3D porosity models. Core data do not exist within the study area. We calculated the total porosity logs (ϕ_t) using the root-mean-square method using the NPHI and DPHI curves. The total porosity logs were upscaled to the cell dimensions and modeled using variogram-based sequential Gaussian simulation. For the Arbuckle Group and shallower formations, the variogram ranges were set to 7000 ft (2134 m) for both horizontal directions and 10 ft (0.6 m) for the vertical direction. Due to the lack of well-log data for the basement, we modeled the porosity distribution in the basement assuming that the porosity for igneous and metamorphic lithologies is in general greater near the faults and essentially zero in nonfaulted areas. This porosity distribution was computed using a “distance-to-object” property using commercial software in which the interpreted fault surfaces are the objects. This

Figure 7. Type log of a GR (to the left) and resistivity and porosity (to the right) showing the major formation tops picked from the Ordovician Arbuckle Group up through the Pennsylvanian Oolagah Limestone showing their ages, as seen on well E. We can see significant contrasts of resistivity and porosity values below the Simpson and Arbuckle Group tops.



approach resulted in porosity values of $\varphi = 6\%$ near fault surfaces and linearly decreasing to $\varphi = 0\%$ 3000 ft away from the fault

Permeability modeling

The porosity models, discussed above and a Buckle's (Buckles, 1965) relationship between calculated irreducible water saturation and porosity constrained the 3D permeability models. Buckle's method estimates the irreducible water saturation, Sw_{irr} , using an empirical relationship between the effective porosity φ_e , the fractional volume of shale V_{sh} , and the Buckle's number κ_{BUCKLE} :

$$Sw_{irr} = \frac{\kappa_{BUCKLE}}{\varphi_e(1 - V_{sh})}. \quad (1)$$

The term V_{sh} is commonly calculated using the GR log. In our case, V_{sh} was set to be zero to assume only the presence of water.

After irreducible water saturation was estimated, qualitative permeability estimates were calculated using the Tixier equation:

$$\kappa = \left(250 \frac{\varphi_e^3}{Sw_{irr}}\right)^2, \quad (2)$$

and the Timur equation (Tixier, 1949; Timur, 1968):

$$\kappa = \left(100 \frac{\varphi_e^{2.25}}{Sw_{irr}}\right)^2, \quad (3)$$

which are a function of the irreducible water saturation and the total porosity model. Three iterations of this process using equations 2 and 3 were run using $\kappa_{BUCKLE} = 0.01$ for vuggy, $\kappa_{BUCKLE} = 0.005$ for crystalline, and $\kappa_{BUCKLE} = 0.001$ for fractured rocks, corresponding to the three possible rock matrix types. An additional six models were run, assuming 100% water saturation and the absence of any hydrocarbons. A vuggy to fine vuggy matrix was assumed for the Arbuckle Group.

Analysis of the injection data

We investigated the well performance of the 29 disposal wells within the seismic survey area, analyzing the daily injection rates, surface-tubing pressures, and well-completion data. We carefully examined the available data to identify anomalous entries. We either corrected (whenever possible) or removed the anomalous data from further analyses. Completion reports provided the perforation depths for all wells. To perform the analysis at subsurface conditions, we converted the wellhead pressures to bottom-hole pressure using commercial software. This conversion also entailed carrying out sensitivity analyses using salinity, multiphase-flow correlations, and water-injection

temperature to identify any artifacts introduced in this pressure conversion process.

We used the modified-Hall analysis (MHA) described by Izgec and Kabir (2011) to investigate the well performance of the 29 disposal wells. The average ambient pressure around the wells is required to calculate the Hall integrals. Next, we used Silin slope analysis (Silin et al., 2005) to calculate the ambient reservoir pressure. Note that Silin analysis yields reliable results only with injection data within a transient flow regime. We identified the flow regimes using material-balance-time diagnostics plots (Anderson and Mattar, 2004). The material balance time is the ratio between the cumulative injection and the instantaneous injection rates. A log-log plot of the daily injection rate against the material balance time helps diagnose the well-flow regimes. The steady-state regime corresponds to the unit slope in the resulting log-log plot. Ascertaining the onset of the steady-state regime provides a means to identify the appropriate range for pressure and injection data for subsequent MHA.

In MHA, we plot Hall integrals and their derivatives (modified-Hall derivatives) with respect to cumulative injection (Izgec and Kabir, 2011) against the cumulative injection. One can consider the Hall integral as a measure of injection-pressure buildup with time, whereas the modified-Hall derivatives indicate the rate of pressure buildup with incremental injection. In a normal injection scenario, both curves (Hall integrals and the modified-Hall derivatives) will have similar slopes against cumulative injection. Whenever the two curves

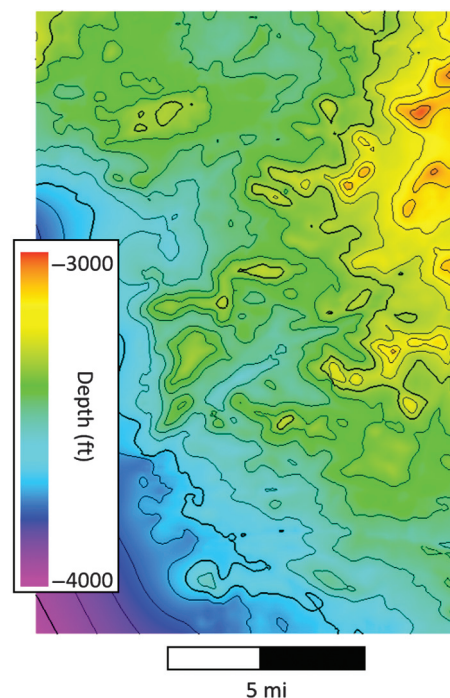


Figure 8. Arbuckle Group structure contour map. The depths increase approximately 1000 ft (approximately 300 m) from northeast to southwest.

deviate away from each other, normal injection ceases. If the slope of the Hall derivatives increases faster than the Hall integral, the well is struggling to inject fluid causing the pressure to build up rapidly. This rapid pressure buildup is an injectivity-loss scenario: for instance, formation plugging and any other kind of formation damage. In contrast, if the slope of the Hall derivatives declines rapidly compared with the Hall integrals, the injected fluid has found a less resistant flow path and the pressure is not building up any further. In fact, the disposal well may experience a pressure decline at this point. This decrease in pressure is a typical disposal well-pressure behavior after formation fracturing has occurred.

We diagnosed the injectivity pattern of all 29 disposal wells using MHA diagnostics explained above. Finally, we formed clusters of wells with similar injection patterns. This provided insights into the history matching of the simulation model discussed next.

History-matching methodology

We considered the Viola, Simpson, Arbuckle Group, and basement formations as flow units in the geologic model. The model has 500×500 ft grid cells, 164 grid points in the x (north), 217 grid points in the y (east), and 185 grid points in the z (vertical) directions, resulting in a 6.5 million cell model that extended laterally approximately $66,500 \times 98,300$ ft. Figure 9 shows the schematic of the simulation model.

After the creation of the major formations, we assigned geologic porosity and permeability parameters to the simulation model. We assigned rock properties based on the type of formations. With respect to the initial fluid distribution, we considered the Arbuckle Group and the basement formations to be water-filled. We modeled completions of all 29 wells according to the available completion reports. In the simulation, we used well injection rates and bottom-hole pressures for the period between January 2005 and May 2016. We included the faults delineated from the seismic interpretation in the simulation models.

We used a Pareto-based history-matching process, first identifying regions of interest for history matching

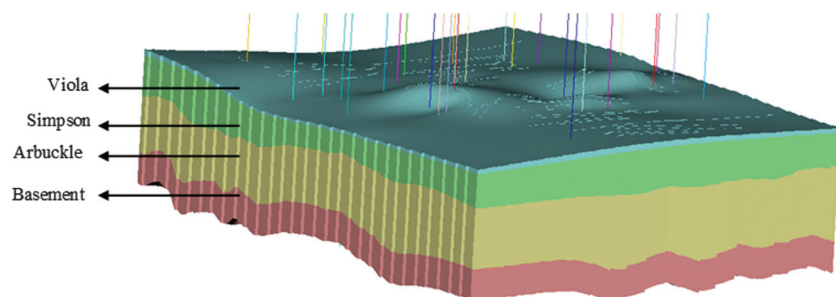


Figure 9. Simulation model schematic showing the four major formations. The 3D grid consists of cells with aerial dimensions of 500×500 ft (152×152 m) and an average layer thickness of 3 ft (0.9 m) resulting in a total of approximately 6.5 million cells.

where the Arbuckle Group Formation is the main disposal zone of interest in our study. We used bottom-hole pressure and injection rates as the model response variables for the history match.

The next step was to identify uncertain parameters for history matching. In this study, we used permeability, horizontal and vertical anisotropy, porosity, and compressibility of the Viola, Simpson, Arbuckle Group and basement formations as the uncertain parameters. We also considered formation-water properties such as the compressibility, viscosity, density, and formation-volume factor to be uncertain. After attaining a moderate history match, we adjusted the injection-well productivity multipliers.

We used reasonably broad ranges for all of the uncertain parameters at the start of history matching. At each stage of history matching, we performed a screening analysis, using Pareto plots to determine those parameters that most impacted the response variables. These key parameters were those associated with the Arbuckle Group Formations and wells. Based on the degree of impact, we adjusted the ranges of the values for subsequent stages of history match. We repeated this process until we obtained an acceptable match of the bottom-hole pressure and the injection rates.

Results

Core and log properties of the Arbuckle Group

Figure 10 displays a type log of the Arbuckle Group showing the primary log curves used in picking the formation tops. From left to right, we display GR, depth, resistivity, porosity, and bulk density tracks. GR values in the Arbuckle range from 25 to 50 API units with a few more clay-rich units near the top of the group with porosities consistently ranging from 5% to 10%.

Top basement structure-contour map including key faults based on seismic data

We analyzed the seismic attributes through the seismic surfaces corresponding to the Arbuckle Group and basement tops. This indicated three major faults from the Arbuckle Group top surface recognized throughout the seismic survey extending into the basement (Figure 11). Fault A, to the north, has an east–west strike orientation, as does Fault C to the south, whereas Fault B has a strike orientation of northwest–southeast. Additional smaller basement faults were interpreted as potential flow barriers.

Arbuckle Group structure-contour and isopach trends based on seismic and well data

Figures 12 and 13 show the interpreted faults for the basement and Arbuckle Group, respectively. The topography appears to be striking at the

same orientation as the middle fault suggesting that the topographic features are controlled by Fault B.

Figure 14 displays an isopach map of the Arbuckle Group. The interval becomes thicker toward the southwest and northwest and has an average thickness of approximately 1200 ft.

3D reservoir model grid (3D stratigraphic and structural framework)

Given the absence of seismic control above the top Arbuckle Formation, we used a simple proportional layering scheme, resulting in a grid containing approximately 6.5 million cells. Figure 15 shows the resulting stratigraphic zones from the basement interval to the top of the Viola Limestone. The basement zone was constructed by creating an arbitrary surface 500 ft (152 m) below the top of the basement surface.

Porosity distribution of the Arbuckle Group and basement

Porosity in the basement ranges between 0.1% and 6%, and log-derived porosity in the Arbuckle

Group ranges between 5% and 10%. For the overlying Simpson group, the porosity is significantly higher (15%–20%), whereas in the shallower Viola Limestone porosity ranges between 0.1% and 5% (Figure 16).

Permeability distribution of the Arbuckle Group and basement

Permeability in the Arbuckle Group ranges between 1 and 5 mD based on the cores discussed previously. Higher permeability exists in the faulted region in the basement and Arbuckle Group ranging between 10 and 100 mD (Figure 17).

Quality control and preconditioning of the injection data

The quality of publicly available data can be debatable. Variation in the reporting formats, changes in the types of measurements and tools, and human errors — all can contribute to significant variation in record-keeping. For this reason, we used a five-step quality control process:

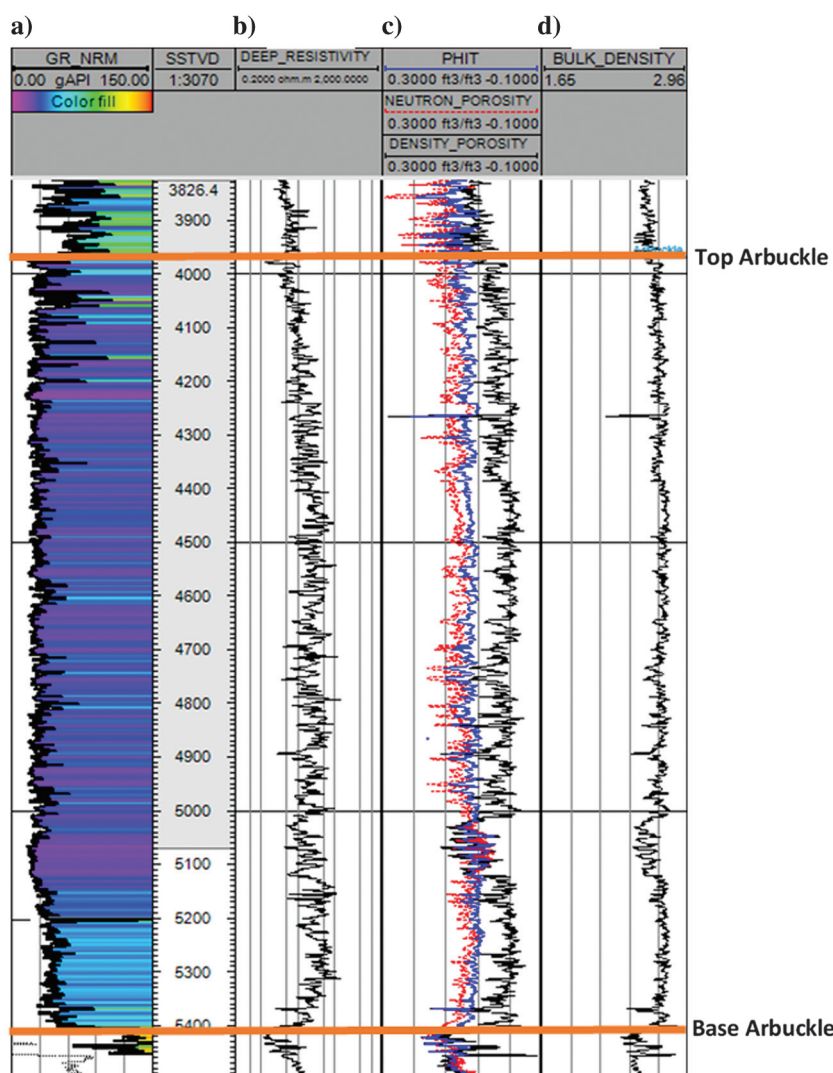


Figure 10. Type log of the Arbuckle Group with the following tracks: (a) GR curve, (b) resistivity, (c) porosity, and (d) bulk density. This well was located outside of the seismic survey, but within the limits of the reservoir model, as can be seen in Figure 14.

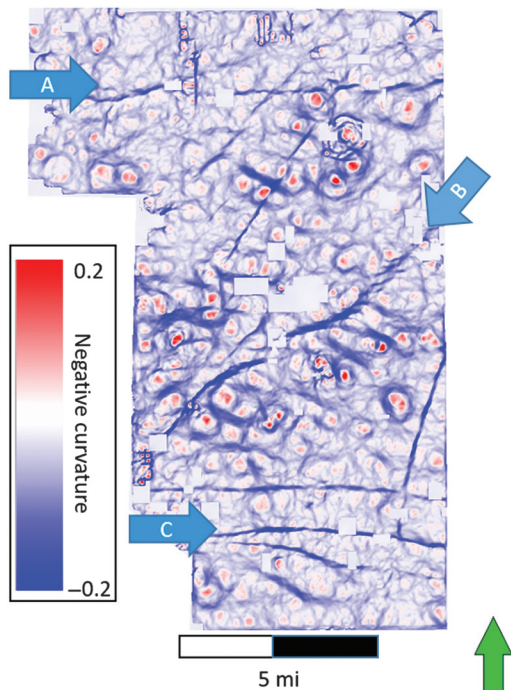


Figure 11. Horizon slice along the top Arbuckle Group through the negative curvature volume showing lineaments corresponding to faults seen on vertical slices through the seismic amplitude volume. Blue arrows indicate three of the larger faults that continue up through the Red Fork Formation (personal communication from the data owner).

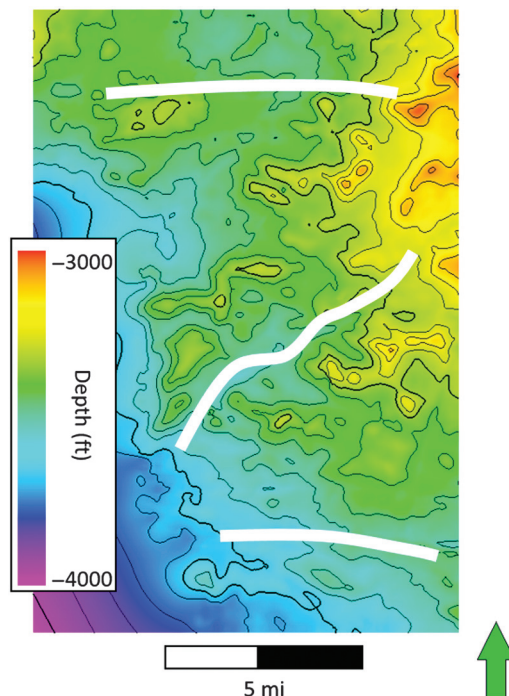


Figure 13. Structure map of the Arbuckle Group top. The white lines represent the location of faults interpreted from curvature attributes.

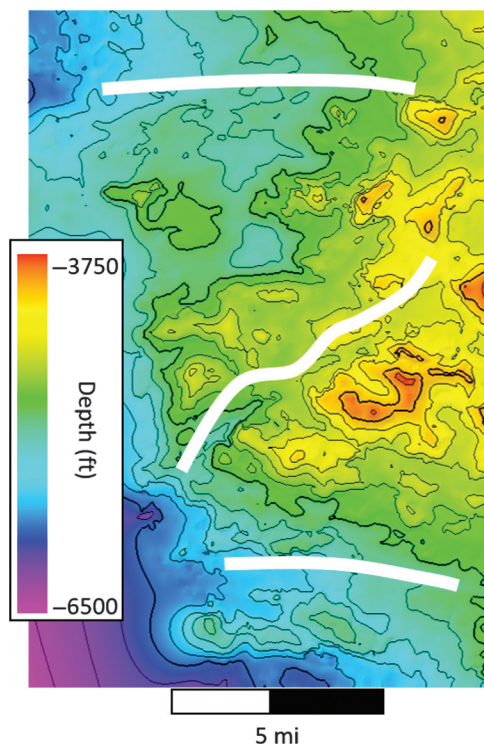


Figure 12. Structure map of the basement top. The white lines represent the location of faults interpreted from curvature attributes.

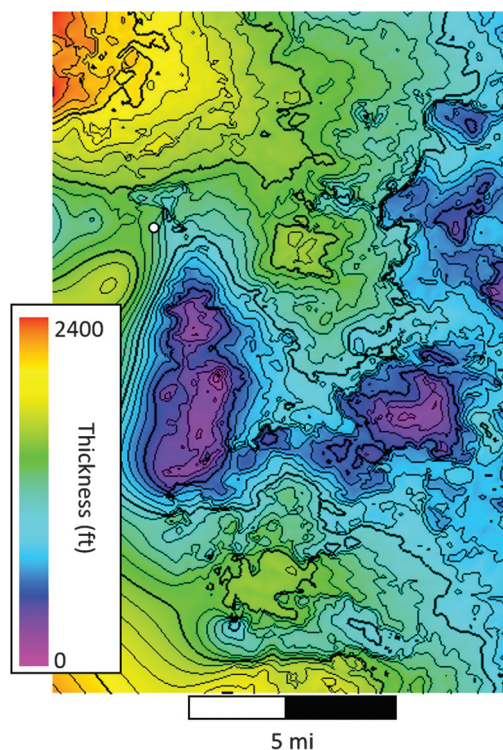


Figure 14. Arbuckle Group Isopach map. The average thickness is approximately 1200 ft (approximately 380 m) for most of the survey with the unit thickening to the southwest and northwest. The white circle represents the location of the type log shown in Figure 10.

Data quality analysis

We first analyzed the pressure and injection-rate data to detect anomalies and rectify them accordingly. Data quality analysis for a random well is shown in Figure 18.

We did not consider pressure data with null records in the study. We also ignored outliers, such as extremely high pressure or injection rates. Possible reasons for

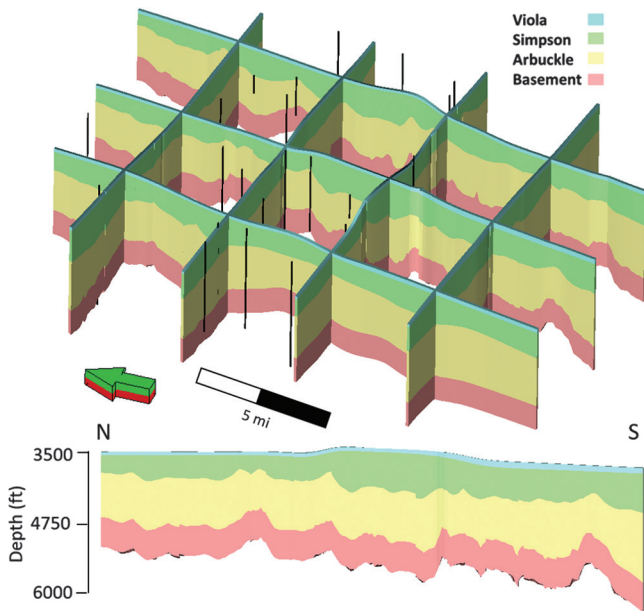


Figure 15. Stratigraphic framework (3D grid). A proportional layering scheme was used, and the resulting grid contains approximately 6.5 million cells. The 3D grid consists of cells with aerial dimensions of 500 × 500 ft (152 × 152 m) and an average layer thickness of 3 ft (0.9 m).

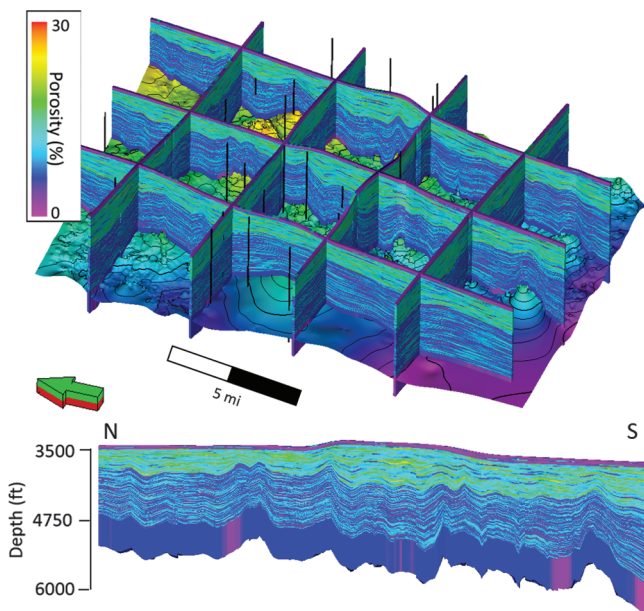


Figure 16. Porosity model of the basement through Viola intervals (vertical magnification 10×).

null records or anomalous data could be erroneous measurements, meters not being operational, lack of calibration, lack of injection, and so forth.

Conversion of wellhead pressures to bottom-hole pressures

For reservoir studies, we require bottom-hole pressure, whereas we measure pressures at the wellhead. We therefore used well-hydraulic correlation models to convert the surface pressure to bottom-hole pressures. Figure 19 shows the results of the pressure conversion for a well.

We conducted sensitivity analysis of the pressure conversion for water salinity, well-hydraulic correlation models, and injection-water temperature. For the base-case pressure conversion, we used a salinity value of 190,000 ppm as recommended by an operator in the region and a water-injection temperature of 60°F.

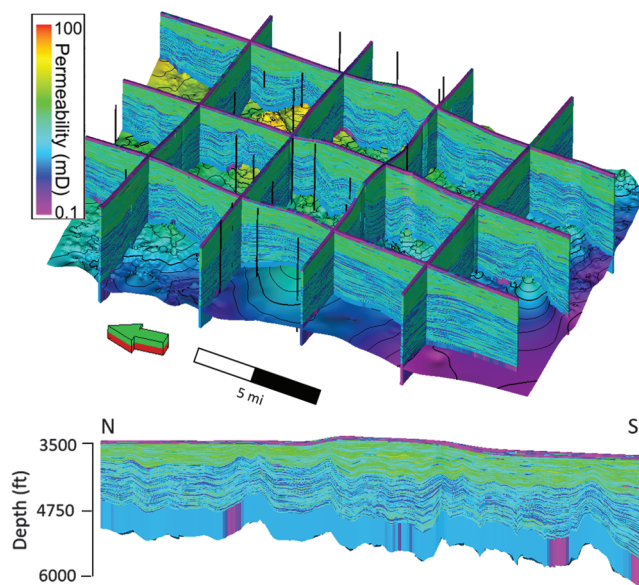


Figure 17. Permeability model of the basement through Viola intervals. Permeability values range from 0.1 to 100 mD, with the highest permeability values being associated with faults interpreted from the seismic survey (vertical exaggeration 10×).

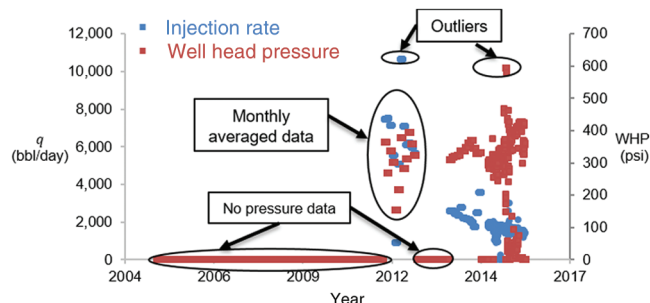


Figure 18. Pressure and injection-rate data for a well highlighting various forms of data quality issues. WHP stands for wellhead pressure.

Flow-regime identification

To analyze the well performance, we first identified the flow regimes to determine the transient or boundary-dominated nature of the injection wells. In the boundary-dominated state, the rates versus material-balance-time curve attains unit slope in a log-log plot. The material balance time is the ratio of the cumulative injection volume and the instantaneous injection rate. Figure 20 shows the material balance time plot of a well indicating the onset of a boundary-dominated state by the dashed line.

Estimation of ambient reservoir pressure

To determine the ambient pressure around the well, we resorted to Silin slope analysis (Silin et al., 2005) because we do not have any other means to determine the pressure at the start of the injection process. Note that such analysis only yields an approximation of the ambient pressure. Additionally, we need early-time transient-state pressure and rate data to determine a reasonable estimate of the ambient pressure. Figure 21 shows the Silin-slope plot for a well.

The slope of the line was found to be 2350 psi, which is the ambient reservoir pressure for this well.

Modified Hall analysis

Figure 22 shows the modified Hall analysis carried out on a well. As evident in the figure, the Hall derivatives increase faster than the Hall integral after a certain

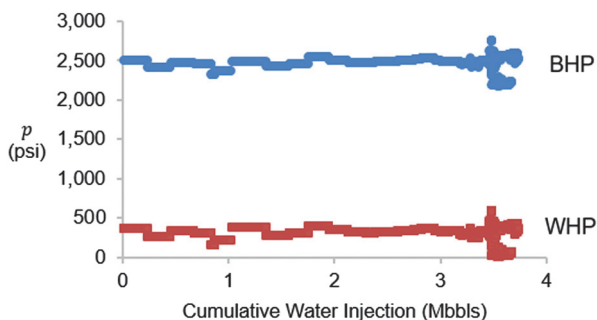


Figure 19. Conversion of wellhead pressure to bottom-hole pressure for a well. BHP stands for bottom-hole pressure.

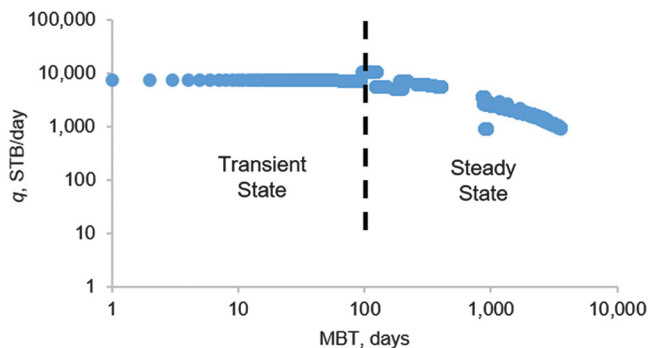


Figure 20. Material-balance-time diagnostics plot of a random well for flow regime identification.

point. It indicates normal injection ceases at this point, and the well is struggling to inject fluid causing the pressure to build up rapidly.

History-matching results

As mentioned previously, we calibrated the simulation model using the observed injection rates and pressure data. Initially, we considered some 50 uncertain parameters through sensitivity runs. The major impactful parameters based on history matching include permeability, porosity, and horizontal and vertical anisotropy of the Arbuckle Group, permeability and horizontal anisotropy of the overlying Simpson and the underlying basement formations, and water density and viscosity. Such an impact of the Arbuckle Group properties is understandable because most of the wastewater injection occurs in the forming formations of this unit, and only a few fault planes intercepting the Arbuckle Group penetrate the overlying Simpson and underlying basement. The Viola Formation properties had little impact on the history-matching process, corroborating the limited number of injection-fluid pathways to reach the Viola Formation.

We carried out multiple stages of history matching, focusing on the key wells and formations. The injection-rate match for most of the wells was good. Figure 23

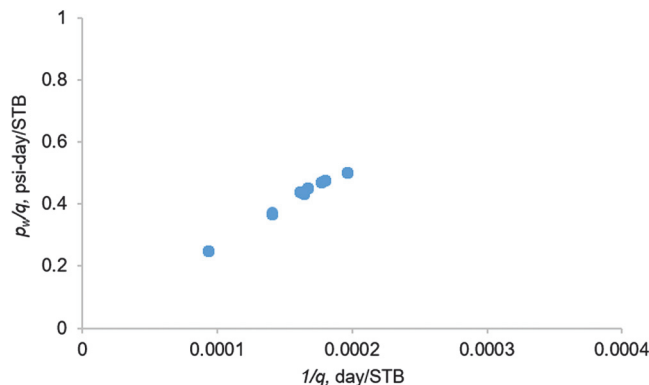


Figure 21. Silin-slope plot.

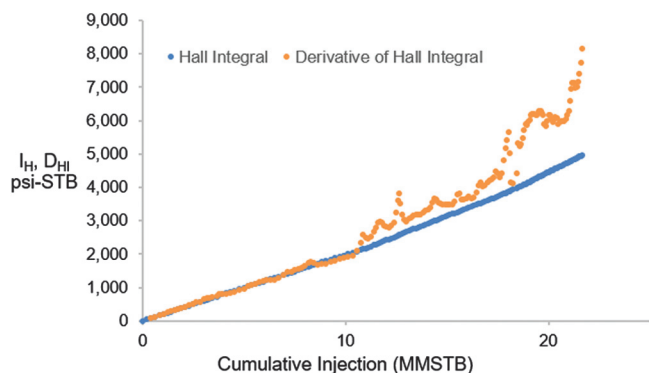


Figure 22. Modified-Hall plot analysis of a well.

presents an aerial view of the wells showing the bottom-hole pressure match where the color coding is based on the percent mismatch. Some of the wells were not used for model calibration because they did not have reliable injection data. These latter wells are color-coded in gray. Green indicates those wells with a pressure mismatch less than 10%, yellow indicates the wells with a mismatch between 10% and 50%, and red indicates wells with a mismatch greater than 50%.

Whereas we are permitted to present the profiles of the bottom-hole pressure and injection rates to validate our scientific analysis, our license agreement does not allow us to disclose actual well names or locations. For the sake of brevity, we only show the bottom-hole pressure and injection rate match for 2 of the 29 wells in Figure 24.

Based on the history match, Tables 1 and 2 present the minimum, maximum, and average porosity and permeability results, respectively, for the Arbuckle Group and Simpson Formations. The average porosity of the Arbuckle Group is approximately 7%, and the average permeability is approximately 10 mD. We observed a slight lateral permeability anisotropy of 1.25 toward the northerly direction with respect to the easterly direction in the Arbuckle Group. We also observed a vertical-to-lateral permeability anisotropy of 0.01. Even though these numbers are different from those initially considered in the initial modeling steps, these were the values that best adjusted to the observed water injection.

Figure 25 displays the simulated pressure distribution in the basement formation in January 2005 and January 2016. Figure 26 shows the distribution of the corresponding pressure buildup due to wastewater injection measured with respect to the initial pressure before the disposal commenced. These figures clearly

indicate pockets of pressure buildup around some of the disposal wells.

We further determined the impact of faults in the Arbuckle Group based on the pressure buildup or the lack of it around the disposal wells. We hypothesize that

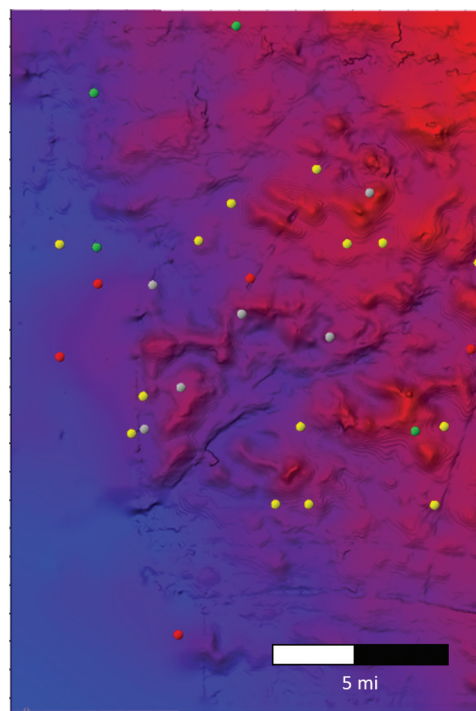


Figure 23. Bottom-hole pressure history-match quality. Color-coded based on mismatch: gray — inconsistent or no data, green — less than 10%, yellow — within 10% and 50%, and red — greater than 50%. In the background, we display the elevation of the Arbuckle Group Formation top: blue represents deeper regions, whereas red represents the shallower regions.

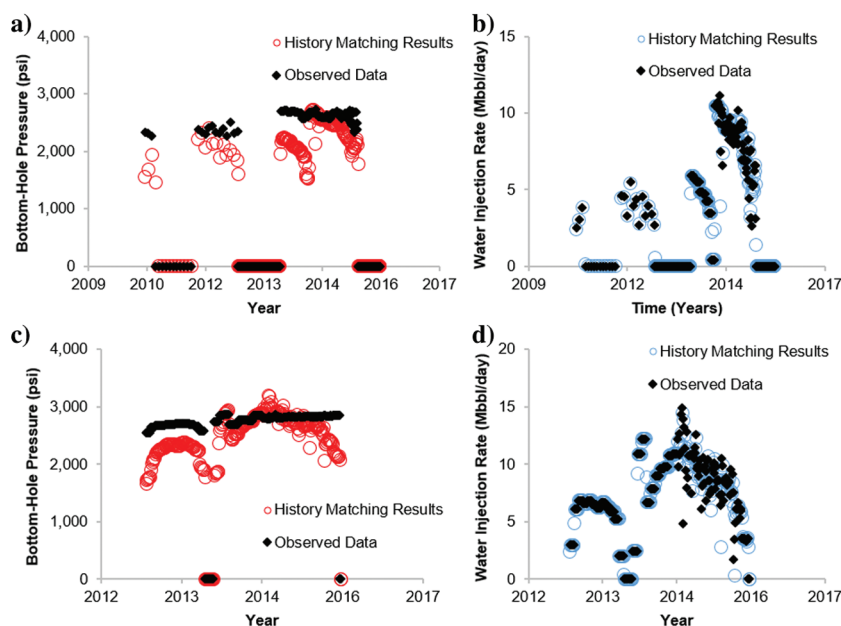


Figure 24. Bottom-hole pressure and injection-rate match for two wells: (a) bottom-hole pressure for well 1, (b) water injection rate for well 1, (c) bottom-hole pressure for well 2, and (d) water injection rate for well 2.

some of the faults may be acting as seals, whereas others may be acting as conduits. However, to conclusively verify the hypothesis, we will need further investigation. Based on the history-match results, we propose the working hypotheses (refer to Figure 27):

- The recorded injection pressure in the wells around the faults F1–F4 was too high. Global and layer-wise adjustments of the history-match parameters in the numerical simulation models could not account for such high pressures. The likely explanation for such high pressure could be (1) incorrect reporting of the pressures, (2) poor storage efficiency of the disposal formation in this area, or (3) these faults are sealing in nature.
- The seismic survey did not extend into the shaded area marked as R1; therefore, it was not possible to identify faults in this region. However, history-

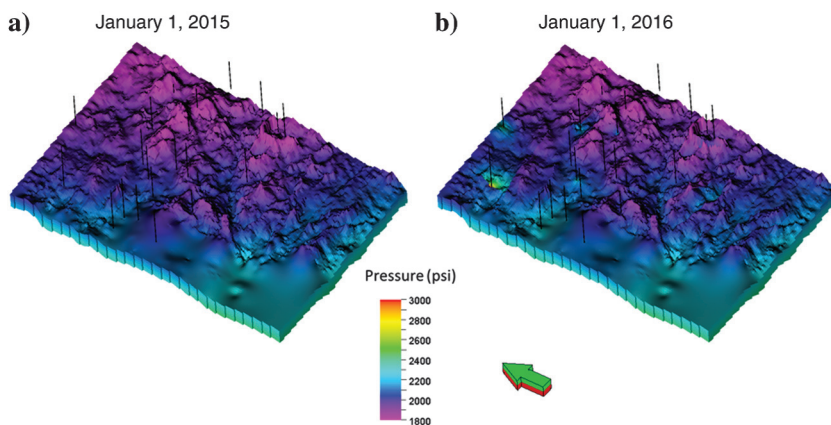
Table 1. Minimum, maximum, and average porosity values for the Arbuckle and Simpson Formations based on history matching.

Formation	Minimum porosity (%)	Maximum porosity (%)	Average porosity (%)
Arbuckle Group	3	15	7
Simpson	2	22	12

Table 2. Minimum, maximum, and average permeability values for the Arbuckle and Simpson Formations based on history matching.

Formation	Minimum permeability (mD)	Maximum permeability (mD)	Average permeability (mD)
Arbuckle Group	1	40	10
Simpson	1	130	40

Figure 25. Distribution of pressure in the basement formation at the (a) beginning of 2005 and (b) beginning of 2016.



match results for several wells in this area indicate the possibility of sealing faults nearby.

Limitations

- Compatibility of injection water and in situ formation water was not investigated. We assumed full compatibility between injection water and formation water (same thermophysical properties). If fluid incompatibility were to be considered, we would expect a higher resistance to flow, which would lead to higher pressure buildup due to injection.
- There was no control on the initial fluid distribution in the disposal zone. In this study, we assumed it to be an aquifer (completely water saturated). We would expect that a multiphase fluid-distribution model would show capillary trapping or residual trapping. This means more resistance to flow, which would translate into higher pressure buildup.
- We did not account for geomechanical stress and strain changes, which may lead to fault reactivation, different pressure, and stress propagation due to injection, among others.

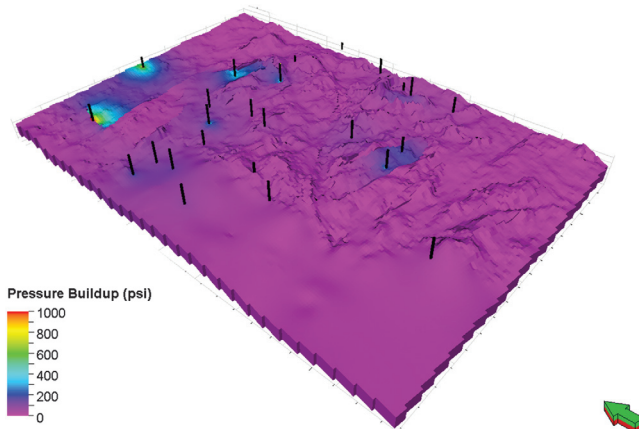


Figure 26. Distribution of pressure buildup due to wastewater injection in the basement formation at the beginning of 2016.

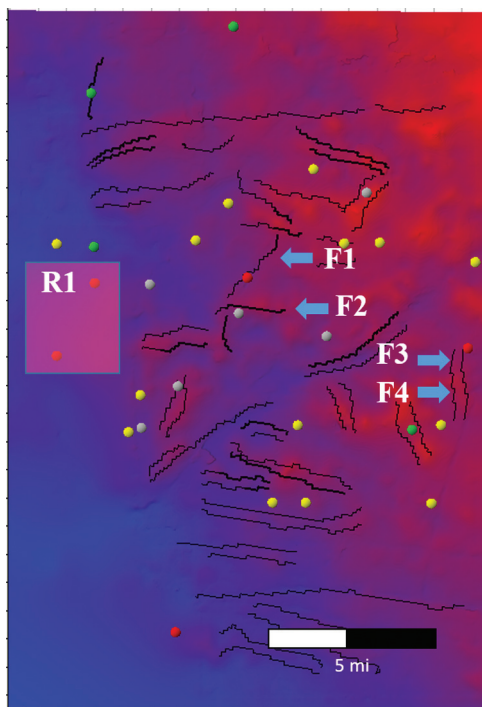


Figure 27. Significance of the interpreted faults based on pressure buildup around the disposal wells. Wells are color-coded according to the quality of the pressure match as used in Figure 23. In the background, we display the elevation of the Arbuckle Group Formation top: Blue represents deeper regions, whereas red represents shallower regions.

- We did not use well hydraulic modeling. Therefore, the back pressure in the well is not accounted for.
- We did not account for communication between any producing interval and the disposal zones. If there is communication, we expect a lower pressure increase due to injection.

Conclusion

In an attempt to better understand the occurrence of basement earthquakes, we used well-established reservoir characterization workflows to construct an integrated characterization study of the Arbuckle Group-basement wastewater disposal system. The Arbuckle Group average porosity is approximately 7%. The corresponding permeability averages approximately 10 mD, with a lateral permeability anisotropy of 1.25. The Arbuckle Group vertical-to-lateral permeability anisotropy is $k_v/k_h \approx 0.01$ for the Arbuckle Group.

The dominant parameters affecting history matching are the porosity as well as the horizontal and vertical permeability of the Arbuckle Group, the permeability and the horizontal anisotropy of the overlying Simpson and the underlying basement formations, the formation water density and the viscosity, and productivity index multipliers of the injection wells. Faults play an important role in fluid movement within the Arbuckle Group

and basement formations. We observed pockets of non-uniform and large pressure buildup in these formations.

Given the public sensitivity to seismicity, operators should consider characterizing their disposal reservoirs in a manner similar to their hydrocarbon reservoirs. This study shows the need for improved data recording and additional data collection. In particular, we recommend that operators wishing to pursue the reservoir characterization analysis used here record their injection data on a daily rather than on a monthly or quarterly averaged basis. Although disposals wells are considered to be an costly, a more quantitative estimation of reservoir properties requires the acquisition of P-wave and dipole sonic logs in addition to the commonly acquired triple-combo logs. Finally, to better quantify flow units with the disposal reservoir, we recommend that operators acquire sufficient core to represent the reservoir heterogeneity.

Acknowledgments

This project was funded as part of the Seismicity Emergency Collaboration project by the State of Oklahoma and coordinated by the Oklahoma Geologic Survey. The authors wish to acknowledge their colleagues in other parts of the larger research project, specifically K. Murray who coordinated our phase of the project fitting into a larger study of groundwater injection throughout Oklahoma. Raster images of the well-log data used in this project were provided by IHS. Well-head pressures were converted to bottom-hole pressure using the commercial software PROSPER. Most of the data interpretation and integration, as well as flow simulation, was conducted using Schlumberger software (Petrel, ECLIPSE, and PIPESIM) provided to the University of Oklahoma for use in research and education. Most importantly, we acknowledge the anonymous oil company operator who wished to further the scientific understanding of the linkage between injection wells and fluid flow near the basement that provided a license to the seismic data volume, initial horizon picks, injection data, and pressure data that were key to conducting this unique research effort.

Data and materials availability

Seismic data is confidential and cannot be released, but well waste water injection data is available through the OGS and OCC respective websites

References

- AASPI, 2017, Attribute-assisted seismic processing and interpretation software documentation, <http://mcee.ou.edu/aaspi/documentation.html>, accessed 26 November 2017.
- Anderson, D., and L. Mattar, 2004, Practical diagnostics using production data and flowing pressures: Presented at the SPE Annual Technical Conference and Exhibition, SPE-89939-MS, doi: [10.2118/89939-MS](https://doi.org/10.2118/89939-MS).
- Bahorich, M. S., and S. L. Farmer, 1995, 3D seismic discontinuity for faults and stratigraphic features: The

- coherence cube: The Leading Edge, **14**, 1053–1058, doi: [10.190/1.1437077](https://doi.org/10.190/1.1437077).
- British Columbia Oil and Gas Commission, 2011, Investigation of observed seismicity in the Horn River Basin, www.bcogc.ca/node/8046/download?documentID=1270, accessed 31 January 2019.
- Buckles, R. S., 1965, Correlating and averaging connate water saturation data: Journal of Canadian Petroleum Technology, **9**, 42–52.
- Chopra, S., L. Infante-Paez, and K. J. Marfurt, 2018, Intra-basement intrusions in the STACK area of Oklahoma: AAPG Explorer, May Geophysical Corner, <https://explorer.aapg.org/story/articleid/46763/intra-basement-intrusions-in-the-stack-area-of-oklahoma>, accessed 3 January 2019.
- Chopra, S., and K. J. Marfurt, 2007, Seismic attributes for prospect identification and reservoir characterization: SEG Geophysical Developments 11, 464.
- Clark, C. E., and J. A. Veil, 2009, Produced water volumes and management practices in the United States, United States Department of Energy, Argonne National Laboratory ANL/EVS/R-09/1, www.evs.anl.gov/pub/doc/ANL_EVS_R09_produced_water_report_2437.pdf, accessed 26 January 2019.
- EIA, 2019, Petroleum and other liquids for the state of Oklahoma, <https://www.eia.gov/dnav/pet/hist/LeafHandler.ashx?f=M&n=PET&s=MCRFPOK1>, accessed 3 January 2019.
- Elebiju, O. O., S. Matson, G. R. Keller, and K. J. Marfurt, 2011, Integrated geophysical studies of the basement structures, the Mississippi chert, and the Arbuckle Group of Osage County region, Oklahoma: AAPG Bulletin, **95**, 371–393, doi: [10.1306/08241009154](https://doi.org/10.1306/08241009154).
- Evans, D. M., 1966, The Denver area earthquakes and the Rocky mountain arsenal disposal well: Mountain Geologist, **3**, 23–26.
- Friberg, P., A. Besana-Ostman, and G. M. Dricker, 2014, Characterization of an earthquake sequence triggered by hydraulic fracturing in Harrison County, Ohio: Seismological Research Letters, **85**, 1295–1307, doi: [10.1785/0220140127](https://doi.org/10.1785/0220140127).
- Gogri, M., 2018, Investigation and real-time monitoring for safe waste-water disposal with a focus on Arbuckle Group, Oklahoma: M.S. thesis, University of Oklahoma.
- Holland, A., 2013, Earthquakes triggered by hydraulic fracturing in south-central Oklahoma: Bulletin of the Seismological Society of America, **103**, 1784–1792, doi: [10.1785/0120120109](https://doi.org/10.1785/0120120109).
- Horton, S., 2012, Disposal of hydrofracking waste fluid by injection into subsurface aquifers triggers earthquake swarm in central Arkansas with potential for damaging earthquake: Seismological Research Letters, **83**, 250–260, doi: [10.1785/gssrl.83.2.250](https://doi.org/10.1785/gssrl.83.2.250).
- Izgec, B., and S. Kabir, 2011, Identification and characterization of high-conductive layers in waterfloods: SPE Reservoir Evaluation & Engineering, **14**, 113–119, doi: [10.2118/123930-PA](https://doi.org/10.2118/123930-PA).
- Jacobs, T., 2016, Seismic shifts in Oklahoma lead to stricter regulations: Journal of Petroleum Technology, **68**, 44–48, doi: [10.2118/0516-0044-JPT](https://doi.org/10.2118/0516-0044-JPT).
- Johnson, K. S., 1991, Geologic overview and economic importance of Late Cambrian and Ordovician rocks in Oklahoma, in K. S. Johnson, ed., Late Cambrian-Ordovician geology of the southern Midcontinent, 1989 Symposium: Oklahoma Geological Survey Circular 92, 3–14.
- Kim, W., 2013, Induced seismicity associated with fluid injection into a deep well in Youngstown, Ohio: Journal of Geophysical Research, **10**, 3506–3518.
- Kolawole, F., C. Johnston, J. Chang, K. J. Marfurt, Z. Reches, and B. M. Carpenter, 2018, Characterization of pre-existing structures in the basement of Oklahoma with implications for induced seismicity: GSA Annual Meeting, Indiana Paper No. 158-6.
- Liao, Z., H. Liu, Z. Jiang, K. J. Marfurt, and Z. Reches, 2017, Fault damage zone at subsurface: A case study using 3D seismic attributes and a clay model analog for the Anadarko Basin, Oklahoma: Interpretation, **5**, no. 2, T143–T150, doi: [10.1190/INT-2016-0033.1](https://doi.org/10.1190/INT-2016-0033.1).
- Matson, S. E., 2013, Mississippi lime play: From outcrop to subsurface — The evolution of a play: Annual Convention and Exhibition, AAPG, Abstract, Search and Discovery Article #110170.
- McGarr, A., B. Bekins, N. Burkhardt, J. Dewey, P. Earle, W. Ellsworth, S. Hickman, A. Holland, E. Majer, J. Rubinstein, and A. Sheehan, 2015, Coping with earthquakes induced by fluid injection: Science, **347**, 830–831, doi: [10.1126/science.aaa0494](https://doi.org/10.1126/science.aaa0494).
- Murray, K. E., 2015, Class II saltwater disposal for 2009–2014 at the annual-, state-, and county-scales by geologic zones of completion, Oklahoma: Oklahoma Geologic Survey Open-File Report OF5-2015.
- Oklahoma Corporation Commission, 2017, Oil and gas info, https://apps.occeweb.com/RBDMSWeb_OK/OCCOOnline.aspx, accessed 10 January 2017.
- Pickett, A., 2018, Oil and Gas Reporter, New Play Concept ‘Merges’ SCOOP and STACK Trends in Red-Hot Central Oklahoma, <https://www.aogr.com/magazine/cover-story/new-play-concept-merges-scoop-and-stack-trends-in-red-hot-central-oklahoma>, accessed 3 January 2019.
- Qi, X., and K. J. Marfurt, 2017, Volumetric aberrancy to map subtle faults and flexures: Interpretation, **6**, no. 2, 1M–Y1.
- Silin, D. B., R. Holtzman, and T. W. Patzek, 2005, Monitoring waterflood operations: Hall method revisited: SPE Western Regional Meeting, SPE-93879-MS, doi: [10.2118/93879-MS](https://doi.org/10.2118/93879-MS).
- Stringer, C. P., 1958, Subsurface geology of Western Payne County, Oklahoma: Shale Shaker Digest II v. VI–VIII.
- Timur, A., 1968, An Investigation of Permeability, Porosity and Residual Water Saturation Relationships for Sandstone Reservoirs: The Log Analyst, **9**, 3–5.
- Tixier, M. P., 1949, Evaluation of permeability from electric-log resistivity gradients: Oil and Gas Journal, **16**, 113.

- Tulsa World, 2019, Oklahoma earthquakes decrease for 3rd straight year, <https://www.apnews.com/216ddc7f8391467c90bd526696beb4f3>, accessed 3 January 2019.
- U.S. Geological Survey, 2019, Do all wastewater disposal wells induce earthquakes?, https://www.usgs.gov/faqs/do-all-wastewater-disposal-wells-induceearthquakes?qt-news_science_products=0#qtnews_science_products, accessed 20 February 2019.
- van der Baan, M., and F. J. Calixto, 2017, Human-induced seismicity and large-scale hydrocarbon production in the USA and Canada: Geochemistry, Geophysics, Geosystems, **18**, 2467–2485, doi: [10.1002/ggge.v18.7](https://doi.org/10.1002/ggge.v18.7).
- Walsh, F. R., and M. D. Zoback, 2015, Oklahoma's recent earthquakes and saltwater disposal: American Association for the Advancement of Science, **1**, 1–9.
- Walters, R., M. Zoback, J. Baker, and G. Beroza, 2015, Characterizing and responding to seismic risk associated with earthquakes potentially triggered by saltwater disposal and hydraulic fracturing: Seismological Research Letters, **86**, 1110–1118, doi: [10.1785/0220150048](https://doi.org/10.1785/0220150048).
- Zoback, M. D., 2010, Reservoir geomechanics: Cambridge University Press, 505.



Gabriel L. Machado received an engineering degree in geophysics from the University Simon Bolivar in Venezuela and an M.S. in geophysics from the University of Oklahoma. He is currently a Ph.D. candidate at the University of Oklahoma. His research interests include seismic attributes and integration of earth science disciplines

to better understand and characterize the subsurface.



Garrett J. Hickman received an M.S. in geology from the University of Oklahoma and is currently employed by the Earth Science Agency in Frederick, Colorado, USA.



Maulin P. Gogri received a bachelor's degree from the Pandit Deendayal Petroleum University (PDP) and a master's degree from the University of Oklahoma (OU) in petroleum engineering. He is currently enrolled at Georgia Tech University for a master's degree in computer science. He is currently working as an AI

researcher at American Water. He has around six years of work experience. Previously, he worked at dataVedik as a petroleum engineer and at Larsen & Toubro (L&T), India, as a process and commissioning engineer.



Kurt J. Marfurt is a research professor of geophysics at the University of Oklahoma and leads the Attribute-Assisted Seismic Processing and Interpretation consortium with the goal of developing and calibrating new seismic attributes to aid in seismic processing, seismic interpretation, and data integration using interactive and machine learning tools. His experience includes 23 years as an academician and 18 years in technology development at Amoco's Tulsa Research Center. He served as the 2006 EAGE/SEG and as the 2018 SEG Distinguished Short Course Instructor. He has taught continuing education short courses for SEG and AAPG since 2003. From 1984 to 2013, he has served as either an associate or assistant editor for *GEOPHYSICS*. In 2013, he joined the editorial board of the SEG/AAPG journal *Interpretation*, where he served as the editor-in-chief for the period 2016–2018, and now serves as deputy editor-in-chief for the period 2019–2021.

Position statement

As a candidate for Director at Large, I note the following challenges facing the SEG:

- **Continuing education:** Given today's learning styles and a desire to balance their professional and personal lives, relatively few young professionals attend local meetings and read journal articles, preferring "just in time" learning that can be immediately applied to the task at hand. SEG needs to become the hub for online interactive geophysical learning.
- **Publications:** In 2018, 62% of the papers submitted and most of our reviewers for *Interpretation* were from outside North America. Many of our most talented geoscientists have never published a scientific paper. SEG needs to construct and continually update online resources to enable these contributors to better share their expertise and findings with the membership at large.
- **Connection:** Members outside the larger oil patches often feel disconnected from the SEG. Even with an active local society, there may only be one or two colleagues with the same expertise and interests. SEG needs to embrace a world of blogs and online communities, where examples, findings, suggested workflows, as well as alternative hypotheses and interpretations can be posted and discussed.



Matthew J. Pranter received a B.S. in geology from Oklahoma State University, a B.S. in geologic engineering from Colorado School of Mines, an M.S. in geology from Baylor University, and a Ph.D. in geology from the Colorado School of Mines. He holds the Lew and Myra Ward Endowed Chair in reservoir characterization

and is a professor of geology and geophysics at the University of Oklahoma. He was previously a geology professor at the University of Colorado at Boulder and a senior research/reservoir geologist with ExxonMobil Upstream Research Company and Conoco. His research interests include reservoir characterization and modeling, sedimentary geology, and petroleum geology.

Zulfiqar A. Reza received a Ph.D. in petroleum engineering from the University of Alberta. He is an associate professor in the Mewbourne School of Petroleum and Geological Engineering at the University of Oklahoma.

He claims more than 20 years of experience in the oil and gas industry, research, and academia including Schlumberger and Chevron, among others, and a stint as an ECLIPSE reservoir-simulator developer. He contributed to a monograph on production-data integration. His current research interests include conventional- and unconventional-reservoir engineering; enhanced oil and gas recovery; advanced reservoir simulation and simulator development; multiscale, multiphysics modeling; pore-scale modeling; data analytics; field-development planning; wastewater disposal; and uncertainty and risk management.